



ICCM Proceedings

**Proceedings
of the International Conference
on Computational Methods**

(Vol. 7, 2020)

11th ICCM, 9th-12th August 2020

Editors: **G. R. Liu, Nguyen-Xuan Hung**

ICCM2020

Proceedings of the International Conference on Computational
Methods (Vol. 7, 2020)

11th ICCM, 9th-12th August 2020, Virtual Conference

Edited by

G. R. Liu

University of Cincinnati, USA

Nguyen-Xuan Hung

HUTECH University of Technology, Vietnam

Table of Contents

Welcome Message	iii
Committees	iv
Table of Contents	vi
Localisation of fire source in a warehouse using plume-tracing method <i>Zeqi Li, Zhao Tian, Tien-fu Lu, Houzhi Wang</i>	1
Moving Polyhedral Mesh Finite Volume Method for Compressible Flows <i>Masashi Yamakawa, Daichi Tanio, Shinichi Asao, Mitsuru Tanaka, and Kyohei Tajiri</i>	6
Debonding analysis of adhesively bonded pipe joints subjected to combined thermal and mechanical loadings <i>Hong Yuan, Jun Han, Huanliang Zhang, Lan Zeng</i>	17
Numerical Simulation of Incompressible Flows Around a Flat Plate Using Immersed Boundary Method with Pressure Boundary Condition <i>Kyohei Tajiri, Yuki Okahashi, Mitsuru Tanaka, Masashi Yamakawa, Hidetoshi Nishida</i>	32
Effect of Mechanical and Chemical Constraints on Swelling of Polyelectrolyte Gels <i>Isamu Riku, Tomoki Sawada and Koji Mimura</i>	40
Development of the numerical method for simulation of ship motions in regular waves with changing wave direction <i>Kunihide Ohashi</i>	46
Numerical Analysis for Promotion of Concentration Diffusion by Rotational Motion of Circular Object <i>Kohei Ueda, Masashi Yamakawa, Shinichi Asao</i>	52
Simulation of Flow in Pressure Tank of Water Rocket <i>Shinichi Asao, Masashi Yamakawa, and Kento Sawanoi</i>	61
Coupled simulation of Influenza virus between inside and outside the body <i>Kiyota Ogura, Masashi Yamakawa, Shinichi Asao</i>	71
Tensegrity form-finding using measure potential and its influential coefficients on the solution <i>Cho Kyi Soe, Shuhei Yamashita, Katsushi Ijima, and Hiroyuki Obiya</i>	83
Homogenization approach for representative laminate plate using Hsieh-Clough-Tocher element <i>Nguyen Hoang Phuong, Le Van Canh, Ho Le Huy Phuc</i>	91

Automatic Adaptive ES-FE Approach for Limit Load Determination of Engineering Structures <i>Vu Le Hoang, Sawekchai Tangaramvong</i>	109
Convolution quadrature time-domain boundary element method for viscoelastic wave scattering by many cavities in 3-D infinite space <i>Haruhiko Takeda, Takahiro Saitoh</i>	121
Numerical Simulation of Incompressible Flows Around a Rotating Object Using ALE Seamless Immersed Boundary Method with Overset Grid <i>Kyohei Tajiri, Akihiro Urano, Mitsuru Tanaka, Masashi Yamakawa, Hidetoshi Nishida</i>	128
Effect of nano silica on fracture properties and crack extension resistance of high-performance concrete <i>Van Thuc Ngo, Tien Thanh Bui, Thi Cam Nhung Nguyen, Thi Thu Nga Nguyen, Duyen Phong Nguyen, and Thanh Quang Khai Lam</i>	137
A node-based smoothed point interpolation method for coupled hydro-mechanical analysis of geomechanical problems <i>Ashkan Shafee, Arman Khoshghalb</i>	149
Higher-order mixed finite elements for nonlinear analysis of frames including shear deformation <i>Joe Petrolito, Daniela Ionescu</i>	164
Dynamic analysis of a FGM beam with the point interpolation method <i>Chaofan Du, Xiang Gao, Dingguo Zhang, Xiaoting Zhou, Junwen Han</i>	175
Entropy-regularized Wasserstein Distances for Analyzing Environmental and Ecological Data <i>Hidekazu Yoshioka, Yumi Yoshioka, Yuta Yaegashi</i>	192
U-Net-based Surrogate Model for Evaluation of Microfluidic Channels <i>Quang Tuyen Le, Pao-Hsiung Chiu, and Chinchun Ooi</i>	199
Response spectrum method considering specific dominant natural modes of double layer truss domes subjected to earthquake motions <i>Koichiro Ishikawa</i>	209
Intelligent Robust Control based on Reinforcement Learning for a kind of Continuum Manipulator <i>Da Jiang, Zhiqin Cai, Xiaolu Qiu, Haijun Peng, and Zhigang Wu</i>	218
Simulation of metal Grain Growth in Laser Powder Bed Fusion Process using Phase-field Thermal Coupled Model <i>Zhida Huang, Jian Lu, Chong Liu, and Bo Li</i>	228
Improvement of a ceramic head in the design of a total hip arthroplasty <i>Aleksandr Poliakov, Vladimir Pakhaliuk</i>	245

Contact analysis based on a linear strain node-based smoothed finite element method with linear complementarity formulations <i>Yan Li, Junhong Yue</i>	256
Boundary element of B-spline wavelet on the interval <i>Qi Wei, Jiawei Xiang</i>	275
A global sensitivity analysis method for multi-input multi-output system <i>Qiming Liu, Nichen Tong, and Xu Han</i>	280
Contact analysis within the bi-potential framework using cell-based smoothed finite element method <i>Qianwei Chen, Yan Li, Zhiqiang Feng, and Huijian Chen</i>	287
Symmetry and superposition rules proposed to apply in engineering design <i>Janusz Rebielak</i>	307
Author Index	311

Effect of nano-silica on fracture properties and crack extension resistance of high-performance concrete

*Ngo Van Thuc¹, †Bui Tien Thanh², Nguyen Thi Cam Nhung², Nguyen Thi Thu Nga³,
Nguyen Duyen Phong⁴ and Lam Thanh Quang Khai¹

¹Mien Tay Construction University, Vietnam.

²Department of Bridge and Tunnel Engineering, University of Transport and Communications, Vietnam.

³Facility of Technical Fundamental, University of Transport Technology, Vietnam

⁴Department of Underground and Mining Construction, University of Mining and Geology, Vietnam.

*Presenting author: nvthuc34@gmail.com

†Corresponding author: btthanh@utc.edu.vn

Abstract:

Concrete in the curing process will appear microcracks inside. They will grow and be connected to form some obvious cracks due to temperature and load changes during extraction. With the propagation of cracks, the sudden fracture can occur to concrete structures. The paper will evaluate the effect of nano-silica on the fracture properties and crack extension resistance of high-performance concrete during the complete fracture process. The crack extension resistance of high-performance concrete including nano-silica will be calculated based on the softening laws and the results obtained from the three-point bending test of beam samples with a notch according to Rilem's recommendation. In addition, the initial fracture toughness and unstable fracture toughness will be determined to estimate the crack propagation stability. Mechanic properties such as compressive strength, tensile strength, and elastic modulus are also determined to calculations in the model. Finally, the crack extension resistance curves for high-performance concrete are established based on a programming method.

Keywords: fracture, high-performance concrete, nano-silica, crack extension resistance

1. Introduction

The incorporation of nanomaterials into high-performance concrete has been documented, which can significantly improve the mechanical properties and durability of concrete. The use of nanometer-sized silica materials in high-performance concrete is considered a new step compared to silica fume materials (micrometer sizes). Nanometer-sized ultrafine silica particles help trigger pozzolanic reactions, which remove the unstable components of $\text{Ca}(\text{OH})_2$ that produce high-performance pozzolan gel products. For high-performance concrete (HPC) with nano-silica (NS) added, the mechanical properties such as compressive strength, flexural strength, elastic modulus, and stress-deformation characteristics are significantly improved according to Recent studies of the author [1]. In the studies using NS in HPC [2] [3] [4], the influence of nano-silica on the fracture characteristics of concrete was mentioned, but there were no specific studies for evaluation.

According to Mindess [5], fracture mechanics can now be used to design and evaluate concrete structures. According to Ricardo et al. [6], concrete containing silica fume will have better fracture parameters than. Silica fume has the effect of increasing the consistency, improving the C-S-H structure, and increasing the quality of the interface transition zone between mortar and aggregate. Fracture energy, fracture toughness, length characteristics are all developed higher when using silica fume, the brittleness of HPC tends to decrease.

According to Zhang et al. [2], fracture characteristics are essential for the safety and durability of HPC structures. The improvement of pore structures in HPC with chemical and mineral admixtures increases the density of the interface transition zone of mortar and aggregate, thus affecting the fracture properties of concrete. Silica ultrafine particles will help mortar's performance and consistency is higher than, increasing the cohesion between cement particles and aggregate, the fracture characteristic of concrete is also improved significantly. The presence of ultrafine particles will improve the microstructure and change the fracture behavior of concrete.

In recent decades, many researchers have described the crack extension resistance of concrete through typical R and K_R curves such as Hilsdorf and Brameshuber [7], Karihaloo [8], Mai [9], Bazant and Jirasek [10], Planas et al. [11], Reinhart et al. [12], Xu and Reinhart [13], Kumar and Barai [14], Dong et al. [15]. Among them, a proposed method for assessing crack extension resistance according to the K_R curve is based on studies of Reinhart et al. [12], Xu and Reinhart [16] [17] [18]. In the studies of Xu et al., the fundamental relationship between the cohesion force operating in the fictitious crack zone and the K_R crack extension resistance curve for the fracture completely in concrete when considering the cohesive stress along the fictitious zone is considered to be a critical factor.

To understand the fundamental relationship between cohesive stress operating in the virtual crack zone and the crack extension resistance curve K_R for the fracture process of high-performance concrete as well as the influence of nano-silica to the cohesive stress along the fictitious crack zone, the method of assessing the resistance to crack extension under the K_R curve based on stress intensity coefficients and the fictitious model will be used. In this method, the K_R crack resistance is obtained by combining the initial crack toughness K_{Ic}^{ini} , which is the inherent strength of the material against the crack's appearance, with cohesive toughness K_I^C representing the contribution of cohesive stress along the fictitious crack area. The K_R crack extension resistance curve was calculated by equations established based on the softening rule of concrete proposed by Reinhart and Xu [12]. Parameter of fracture characteristics and two load curves - crack mouth extension displacement (P - CMOD), load - deflection (P - δ) of concrete from a three-point bending test following the standard with crevice primer will be used for calculation.

2. Effect of nano-silica to fracture characteristics of high-performance concrete

2.1. Nano-silica

Research using NS product (Aerosil 200) of Evonik chemical company (Belgium) with dimensions from 5-50nm, the typical surface area of $(200 \pm 25)\text{m}^2/\text{g}$. The results of SEM analysis experiments to evaluate nano silica's size and shape are shown in Figure 1. From Figure 1, it can be seen that the nanoparticles are spherical with an average size of about 13nm.

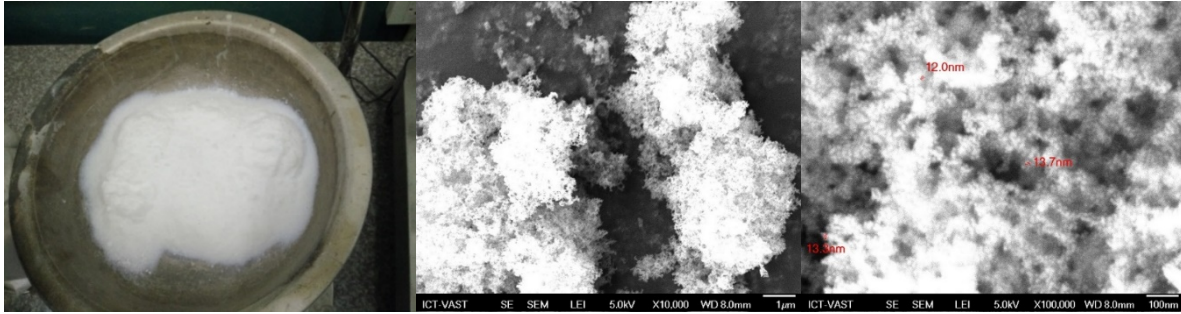


Figure 1. Nano-silica and SEM analysis results

2.2. Prepare the experiment

2.2.1. Mix proportions

HPC contains NS is designed with typical intensity of 70MPa calculated by the ACI method [19]. HPC's composition with 0%, 0.5% and 1.5% NS ratios were used for the fracture characterization test. The percentage of superplasticizer is selected according to the manufacturer's recommendations and is adjusted in practice to ensure the workability of the concrete mixture.

Table 1. Composition of high-performance concrete using nano-silica

Mix code	Material							
	Cement	Fine Aggregate	Coarse Aggregate	SF	NS	SP	Water	W/B
	(kg)	(kg)	(kg)	(kg)	(%)	(lit)	(lit)	
0%NS	544.21	674.68	1049.75	28.64	0.00	5.44	154.67	0.27
0.5%NS	541.34	673.68	1049.75	28.64	0.50	6.53	154.67	0.27
1.5%NS	535.61	671.67	1049.75	28.64	1.50	7.62	154.67	0.27

Note: NS – Nano-silica, SF – Silica fume, SP – Superplasticizer, W/A – Water/Binder.

2.2.2. Manufacturing experimental samples

The study used a three-point bending test of beam samples with a notch to determine the fracture characteristics of concrete according to Rilem's recommendation [20]. The beam sample used in the three-point bending test is a prism of size 500x100x100mm with a 2mm widens of the notch. The notch depth is 25mm, and the ligament area is 100x75mm² (Figure 2).

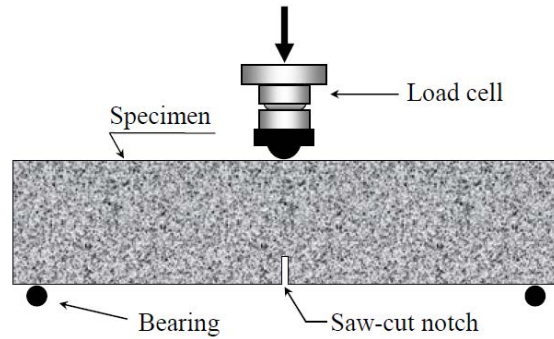


Figure 2. Three-point bending test of the beam sample

All notches are cut on a surface perpendicular to the top of the sample during casting. Test beams after 28 days shall be made the notch on the 21st day. After that, the samples are cured until the day of testing.

2.3. Experimental methods

Experiment with three-point bending beams with the notch used to determine the fracture parameters of concrete, and the test is described as shown in Figure 3. The fracture test is not the same as the strength test or other mechanical properties, load control is not used but instead by controlling displacement or crack mouth opening displacement on the sample. All three-point bending tests are carried out in closed-loop condition, using the Control experiment machine. The parameters measured during the experiment were the load, the displacement of the beam measured by the linear variable differential transformer (LVDT), the crack mouth open displacement (CMOD) was measured by using an extensometer with an experimental layout as shown in Figure 3.

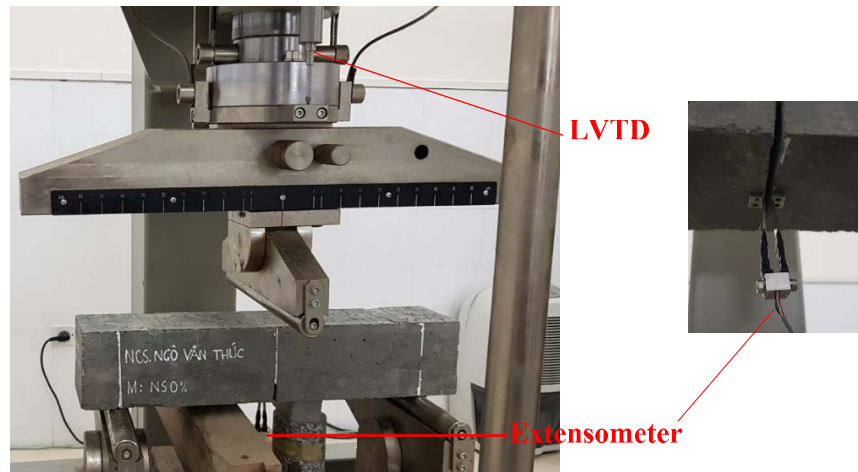


Figure 3. Three-point bending test of HPC beam sample using nano-silica

In RILEM's recommendations [20], it is necessary to conduct experiments so that the rate of increase in mid-span displacement is a constant of 0.2 mm/min. However, the study proposes a small change can be made to this requirement. Instead of performing experiments under mid-span displacement control, the tests were performed under crack mouth open displacement (CMOD) control.

2.4. Experimental results

2.4.1. Effect of nano-silica on the relationship of load and crack mouth open displacement (P - $CMOD$)

The P - $CMOD$ curve of non-NS concrete has a significant slope after reaching the peak (P_{max}), the force value decreases rapidly when the $CMOD$ is very small. When adding nano-silica into the concrete at a rate of 0.5% and 1.5%, the resulting P - $CMOD$ curve has a marked change. In the early stages, the concrete is still in the elastic stage; all samples' curves tend to grow the same, as shown in Figure 4. The difference begins to appear at the stage when the curves are about to peak, the top of the curve of concrete using NS is higher than unused concrete. These can easily understand that the concrete's tensile strength using NS is higher than not using.

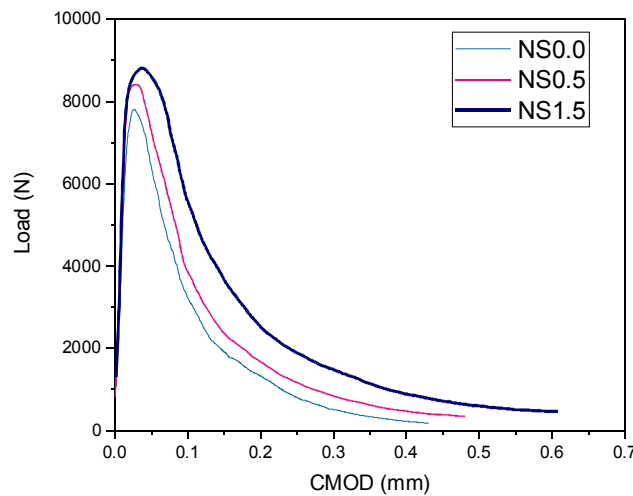


Figure 4. Relationship diagram between load and crack mouth open displacement

Crack mouth open displacement corresponding to P_{max} ($CMOD_c$) of beam samples using 0.5% and 1.5% NS increased compared to control samples (0%), respectively 77.80% and 107.40%. The displacement of cracks widened when the sample was completely destroyed ($CMOD_{max}$) of beam samples using 0.5% and 1.5% NS increase compared to the control sample (0%), respectively 18.75% and 39.31%. From the $CMOD$ results, the contribution of nano-silica particles in minimal amounts can significantly improve the toughness of concrete.

2.4.2. Effect of nano-silica on the relationship between load and deflection (P - δ)

The relationship between the load and deflection (P - δ) of high-performance concrete with additional NS ratios is shown in Figure 5. For the NS-using concrete, the curve P - δ thicker, the nonlinear phase of the curve becomes longer, and the load decreases more slowly.

The displacement between maximum spans (δ_{max}) of the three-point bending test surveyed on the concrete beam, based on Figure 5, can be seen that δ_{max} increases when comparing samples using NS from 0.5% to 1.5 % of the control sample (0% NS).

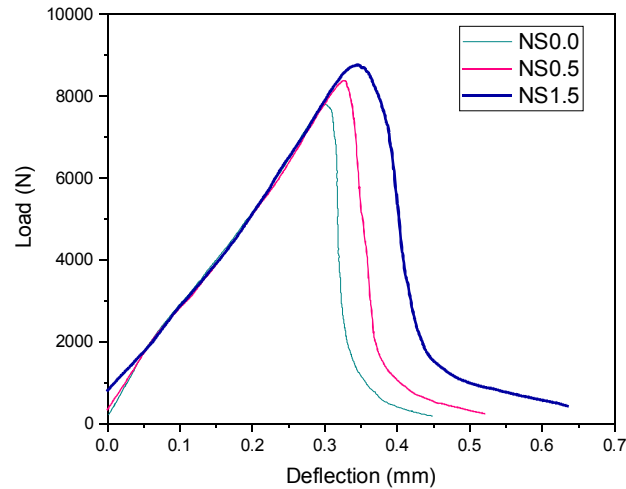


Figure 5. Relationship diagram between load and deflection

Observation Figure 5 shows the change of the relationship curves between the load and deflection in the middle of the span showing that the area under the P- δ curve and the horizontal axis (W_F) of the graph vary in the proportion of NS. Use the integral method to calculate the area under the P- δ curve. The results showed that W_F increased by 21.42% when the NS ratio was 0.5% and 58.71% when the NS ratio was 1.5%.

2.4.3. Effect of nano-silica on fracture energy (G_F)

The change in the value of fracture energy when the ratio of NS varies from 0%, 0.5%, 1.5% is shown in Figure 6. Compared to concrete samples without NS, the beams using NS with fracture energy increased by 21% and 58%, respectively, NS ratio is 0.5% and 1.5% of binder.

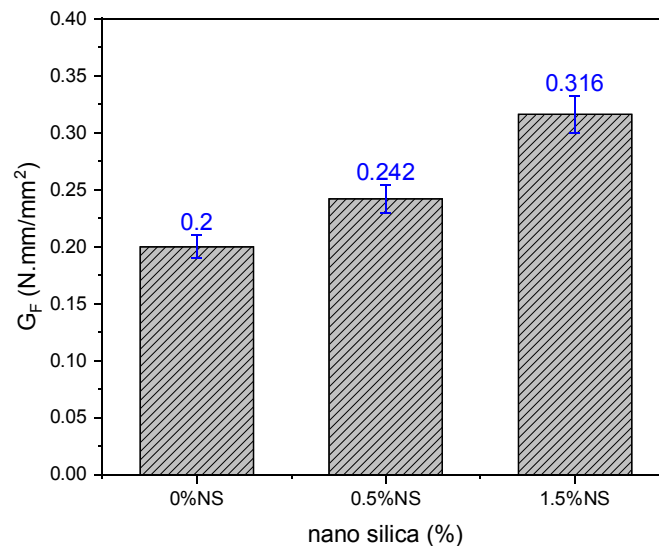


Figure 6. Fracture energy results of HPC using NS

From the G_F results of the gradation of concrete using more NS, it shows that the energy required for fracture is higher.

2.4.4. Effect of nano-silica to characteristic length (l_{ch})

Basing on the characteristic length of the fracture process zone to evaluate the brittleness of high-performance concrete mixes with the change of NS content. This parameter was determined based on the energy parameters of G_F , tensile strength, and elastic modulus. In particular, the tensile strength and elastic modulus were taken from the previous research results of the authors [1]. The result of the calculation is shown in Figure 7.

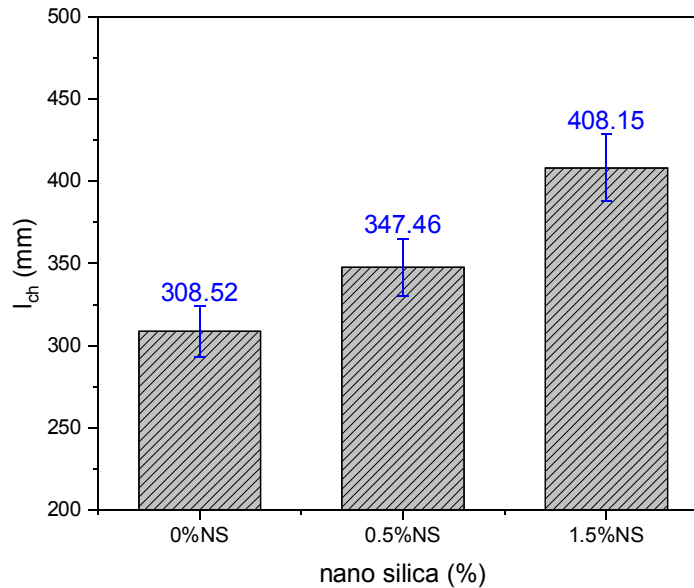


Figure 7. Calculation results of characteristic length

The results of calculating the l_{ch} of the samples using NS are higher than the samples without NS. Based on the assessment, according to the CEB-FIP standard [21]. It can be seen that non-NS concrete is more brittle than aggregate using NS.

3. The crack extension resistance of high-performance concrete using nano-silica

3.1. Approach to calculate the resistance to crack expansion of concrete

To evaluate the effect of nano-silica on the crack extension resistance of concrete, the evaluation method, according to $K_R(\Delta a)$ of Xu et al., is based on the concrete softening law applied [22] [17] [23]. In this method, the K_R crack propagation resistance is obtained by a combination of initial crack toughness K_{Ic}^{ini} , which is the inherent intensity of the material against the occurrence of propaganda cracks, together with, K_I^C is the cohesive toughness of the crack propagation strength due to the contribution of the cohesive stress along the crack propagation zone.

$$K_R = K_{Ic}^{ini} + K_I^C \quad (1)$$

In the finite element calculations for concrete structures based on Hillerborg's cohesive crack model [24], a bilinear softening rule to describe the softening properties of concrete materials was used and widely used by many researchers. The bilinear softening traction-separation law has also been used in the search for analytical expressions of the crack resistance curve [23].

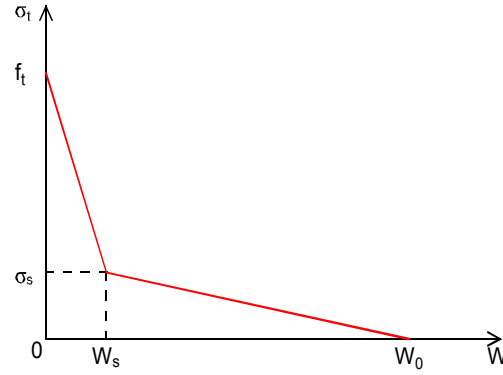


Figure 8. The bilinear softening traction-separation law

According to Xu and Reinhardt [23], the general formula for calculating the cohesion strength for three-point bending test of beams is as follows:

$$K_I^C(\Delta a) = \int_{a_0}^a 2\sigma(x)F_1\left(\frac{x}{a}, \frac{a}{D}\right) / \sqrt{\pi a} dx \quad (2)$$

while:

$$F_1\left(\frac{x}{a}, \frac{a}{D}\right) = \frac{3.52(1-x/a)}{(1-a/D)^{3/2}} - \frac{4.35-5.28x/a}{(1-a/D)^{1/2}} + \left\{ \frac{1.30-0.30(x/a)^{3/2}}{\sqrt{1-(x/a)^2}} + 0.83 - 1.76\frac{x}{a} \right\} \left\{ 1 - \left(1 - \frac{x}{a}\right) \frac{a}{D} \right\} \quad (3)$$

The stages of fracture can be characterized by four different crack propagation sites [52]. The first station is $a = a_0$, and the second is $a_0 \leq a \leq a_c$, the third is $a_c \leq a \leq a_{w0}$ and finally $a > a_{w0}$.

According to the four different stages of crack propagation, the cohesive strength is calculated using the general formula (2). The cohesion stress corresponds to the four crack propagation phases proposed by Xu and Reinhardt [23]:

(a) Case: $a = a_0$

$$\sigma(x) = 0 \quad (4)$$

(b) Case: $a_0 \leq a \leq a_c$

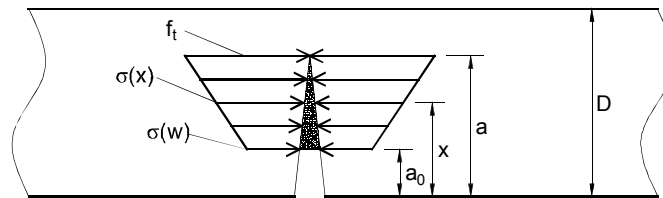


Figure 9. Cohesion stress distribution during crack propagation stage $a_0 \leq a \leq a_c$

Cohesive stress distribution function along the coherent cracking area:

$$\sigma(x) = \sigma(w) + (f_t - \sigma(w))(x - a_0) / (a - a_0) \quad (5)$$

(c) Case: $a_c \leq a \leq a_{w0}$

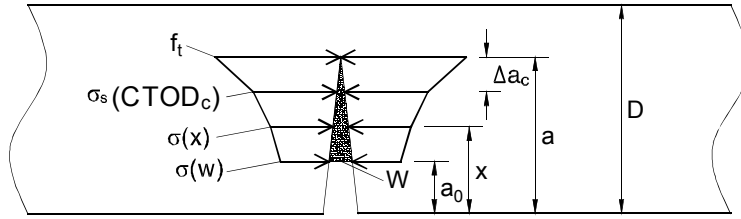


Figure 10. Cohesion stress distribution during the crack propagation stage $a_c \leq a \leq a_{w0}$

Cohesive stress distribution function along the coherent cracking area:

$$\sigma(x) = \begin{cases} \sigma_1(x) = \sigma(w) + [\sigma_s(CTOD_c) - \sigma(w)](x - a_0) / [a - (a_0 + \Delta a_c)] & \text{ khi } a_0 \leq x \leq (a - \Delta a_c) \\ \sigma_2(x) = \sigma_s(CTOD_c) + [f_t - \sigma_s(CTOD_c)](x - a + \Delta a_c) / \Delta a_c & \text{ khi } (a - \Delta a_c) \leq x \leq a \end{cases} \quad (6)$$

(d) Case: $a > a_{w0}$

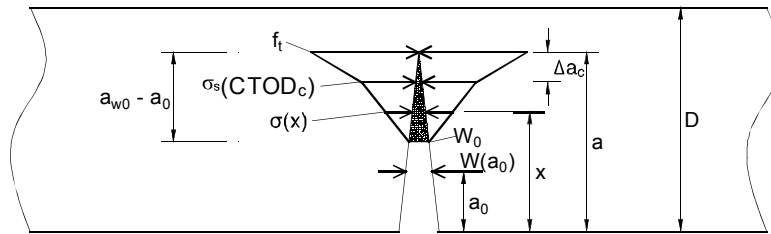


Figure 11. Cohesion stress distribution form during crack propagation stage $a > a_{w0}$

Cohesive stress distribution function along the coherent crack zone:

$$\sigma(x) = \begin{cases} \sigma_1(x) = 0 & \text{ khi } (a_0 \leq x \leq (a - a_{w0} + a_0)) \\ \sigma_2(x) = \sigma_s(CTOD_c)(x - a - a_0 + a_{w0}) / (a_{w0} - a_c) & \text{ khi } (a - a_{w0} + a_0) \leq x \leq (a - \Delta a_c) \\ \sigma_3 = \sigma_s(CTOD_c) + [f_t - \sigma_s(CTOD_c)](x - a + \Delta a_c) / \Delta a_c & \text{ khi } (a - \Delta a_c) \leq x \leq a \end{cases} \quad (7)$$

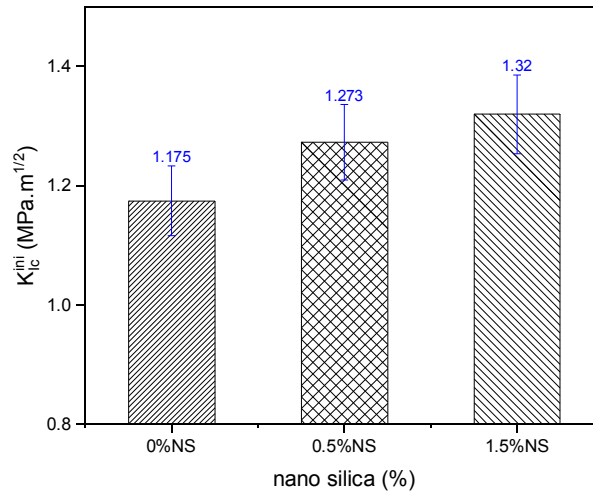
3.2. The result of calculating resistance to crack extension

The sequence of calculations is set in a series programmed by commercial software Mathcad. The fracture parameters and the P - CMOD relationship curve of high-performance concrete using NS obtained from the experiment will be applied to the calculation.

Table 1. Criteria for calculating cracking resistance

Mix code	f_c (MPa)	f_t (MPa)	E (MPa)	G_F (N.mm/mm ²)	W_0 (mm)	H_0 (mm)	S×D×B (mm)
0%NS	82.10	5.43	45533	0.200	0.133	3.0	400×100×100
0.5%NS	84.09	5.76	47620	0.242	0.151	3.0	400×100×100
1.5%NS	87.10	6.23	50131	0.316	0.183	3.0	400×100×100

3.2.1. Initial crack toughness



Hinh 12. Effect of NS to initial crack toughness of HPC

Observe Figure 12, showing that the NS content significantly influences the initial crack toughness of the HPC. When the ratio of NS increases, K_{Ic}^{ini} increases accordingly, indicating that when using NS will help HPC prevent cracks from appearing better.

3.2.2. Cohesive crack toughness

The calculation results of cohesive toughness were base on the crack propagation length Δa is shown in Figure 13.

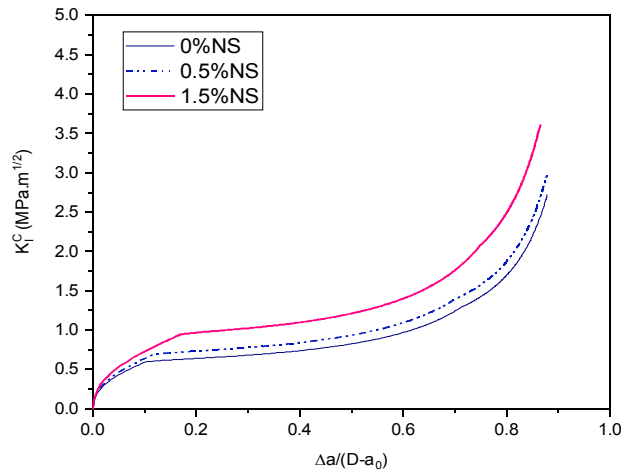


Figure 13. Effect of NS to cohesive crack toughness of HPC

Observe the curves in Figure 13, in the segment after the crack propagation, the values K_I^C corresponding to the crack propagation lengths (Δa) of the HPC using NS are higher than the available type. This change influence of NS to the cohesive characteristic of the surfaces after cracking, which enhances the strength of cohesive.

3.2.3. The crack extension resistance

The crack extension resistance is the result of the combined initial toughness (K_{lc}^{ini}) and cohesive toughness (K_I^C), as shown in Figure 14.

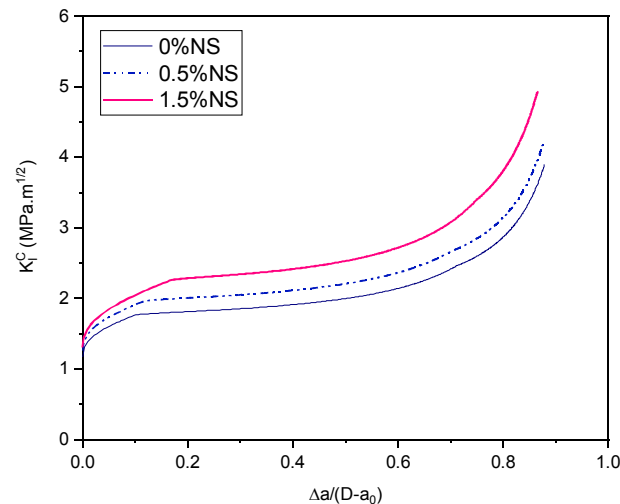


Figure 14. Effect of NS on crack extension resistance in HPC

The curves in Figure 14, clearly show the influence of NS on the crack extension resistance corresponding to the load stage (P) and crack propagation length (Δa). The crack resistance curve corresponding to HPC gradients using 1.5% NS has a starting point that is higher than the other mixture, and the values along the crack are similarly more significant. The results of the cracked resistance curves were observed, showing high similarity to the crack extension resistance curves calculated by other authors [15] [17] [23].

4. Conclusion

The fracture characteristics of high-performance concrete were investigated through the modification of silica nano content in gradients. When using NS in HPC helps improve fracture energy and ductility of HPC. The results show that the level of fracture characteristics are significant, with the ratio of used NS is 1.5%.

Fracture toughness values due to the inherent toughness of the material (initial toughness), the strength caused by the adhesive stress along the crack (cohesive toughness), is improved when using NS in HPC.

The crack extension resistance curve is calculated using Mathcad programming software based on the formulas established based on applying the bilinear softening traction-separation law. The result of the crack resistance of HPC using NS will be higher than the control type. These curves can be used in assessing the crack propagation stability of HPC.

Acknowledgment

The author acknowledges the support by The Laboratory of Department of Underground and Mining Construction, University of Mining and Geology, Vietnam.

References

- [1] Ngo, V.T., Lam, T.Q.K., Do, T.M.D. and Nguyen, T.C. (2020), "Increased plasticity of nano concrete with steel fibers," *Magazine of Civil Engineering* **93**, 27-34.

- [2] Zhang, P., Wan, J., Wang K. and Li, Q. (2017), "Influence of nano-SiO₂ on properties of fresh and hardened high performance concrete: A state-of-the-art review," *Construction and Building Materials* **148**, 648-658.
- [3] Khaloo, A., Mobini, M. H. and Hosseini, P. (2016), "Influence of different types of nano-SiO₂ particles on properties of high-performance concrete," *Construction and Building Material* **113**, 188-201.
- [4] Chithra, S., Kumar S. R. R. and Chinnaraju, K. (2016), "The effect of Colloidal Nano-silica on workability, mechanical and durability properties of High Performance Concrete with Copper slag as partial fine aggregate," *Construction and Building Materials* **113**, 794-804.
- [5] Mindess, S. (2002), "Applications of fracture mechanics to concrete: Where do we go from here?," *Material Science to Application* **206**, 475-485.
- [6] Ricardo, A.E. and Marta, S.L.V. (2006), "Fracture parameters for high-performance concrete," *Cement and Concrete* **36**, 576-583.
- [7] Hilsdorf, H.K. and Brameshuber, W. (1984), "Size effects in the experimental determination of fracture mechanics parameters," *Shah SP, editor. Application of fracture mechanics to cementitious composites. NATO-ARW*, 361-397.
- [8] Karihaloo, B.L. (1987), "Do plain and fiber-reinforced concretes have an R-curve behaviour?," *Shah SP, Swartz SE, editors. Fractures of concrete and rock*, 96-105.
- [9] Mai, Y.W. (1984), "Fracture measurements of cementitious composites," *Shah SP, editor. Application of fracture mechanics to cementitious composites. NATO-ARW*, 399-429.
- [10] Bazant, Z.P. and Jirasek, M. (1993), "R-curve modeling of rate and size effects in quasibrittle fracture," *International Journal of Fracture* **62**, 355-373.
- [11] Planas, J., Elices, M. and Ruiz, G. (1993), "The equivalent elastic crack: 2. X-Y equivalences and asymptotic analysis," *Journal of Fracture* **61**, 231-246.
- [12] Reinhardt, H.W., Cornelissen, H.A.W. and Hordijk, D.A. (1986), "Tensile tests and failure analysis of concrete," *Journal of Structural Engineering, ASCE* **112**, 2462-2477.
- [13] Xu, S. and Reinhardt, H.W. (1999), "Determination of double-K criterion for crack propagation in quasi-brittle materials - part II: analytically evaluating and practically measuring methods for three-point bending notched beams," *International Journal of Fracture* **98**, 151-77.
- [14] Kumar, S. and Barai, S.V. (2008), "Influence of specimen geometry and size-effect on the KR-curve based on the cohesive stress in concrete," *International Journal Fracture* **152**, 127-148.
- [15] Dong, W., Wu, Z.M. and Zhou, X.M. (2013), "Calculating crack extension resistance of concrete based on a new crack propagation criterion," *Construction Building Material* **38**, 879-889.
- [16] Xu, S. and Reinhardt, H.W., "Crack extension resistance and fracture properties of quasi-brittle materials like concrete based on the complete process of fracture," *International Journal of Fracture* **92**, 71-99.
- [17] Xu, S. and Reinhardt, H.W. (1998), "Crack extension resistance and fracture properties of quasi-brittle softening materials like concrete based on the complete process of fracture," *complete process of fracture* **92**, 71-99.
- [18] Reinhardt, H.W. and Xu, S. (1999), "Crack extension resistance based on the cohesive force in concrete," *Engineering Fracture Mechanics* **64**, 563-587.
- [19] ACI 211.4R-08 (2008), Guide for Selecting Proportions for High-Strength Concrete Using Portland Cement and Other Cementitious Materials, *American Concrete Institute*.
- [20] RILEM (1985), "Determination of the fracture energy of mortar and concrete by means of three-point bend tests on notched beams," *Materials and Structures* **18**, 285-290.
- [21] Fib (2008), Constitutive modelling Constitutive modelling high performance concrete, Stuttgart: *Task Group 8.2*.
- [22] Xu, S. and Reinhardt, H.W. (1998), "Crack extension resistance and fracture properties of quasi-brittle materials like concrete based on the complete process of fracture," *International Journal of Fracture* **92**, 71-99.
- [23] Reinhardt, H.W. and Xu, S. (1999), "Crack extension resistance based on the cohesive force in concrete," *Engineering Fracture Mechanics* **64**, 563-587.
- [24] Hillerborg, A. (1976), "Analysis of crack formation and crack growth in concrete by means of fracture mechanics and finite elements," *Cement and Concrete Research* **6**, 773-782.